# Supporting Information

## Schlegel et al. 10.1073/pnas.1115796109

### SI Materials and Methods

**Organisms and Cultivation.** *Methanosarcina acetivorans* (1) WWM1 [C2A, Δhpt (2)] was kindly provided by Michael Rother, Department of Molecular Microbiology and Bioenergetics, Goethe University Frankfurt am Main, Germany, and grown in single-cell morphology (3) at 37 °C in high-salt medium (4) containing either 150 mM methanol or 120 mM acetate as sole carbon and energy source. The $Na_2S{\cdot}9H_2O$ concentration was raised to 0.15 g/L. Growth conditions were strictly anaerobic under an atmosphere of $N_2/CO_2$ (80:20, vol/vol) in 10 or 20-L anaerobic fermenters (Ochs). The growth was measured by measuring the optical density at 578 nm ($OD_{578}$) using a Hitachi U-1800 spectrometer.

**Preparation of Membrane Vesicles.** The harvest and preparation of vesicles was strictly anaerobic under an atmosphere of $N_2$. Cells were grown to $A_{578}$ of 0.6–0.8 and harvested at 13,000 rpm at 4 °C with a flow-through centrifuge (Heraeus Contifuge, Stratos, HCT 22.300 rotor). Cells were washed twice (11,350 × *g*, 15 min, 4 °C) with a buffer containing 2 mM potassium phosphate (pH 7) and 10 mM $NH_4Cl$, 20 mM $MgSO_4{\cdot}7H_2O$, 2 mM $CaCl{\cdot}H_2O$, 0.4 M sucrose, 10 mM DTE, and 1 mg/L resazurin. The cells were then resuspended in 30 mL of the same buffer. To remove the S-layer, the cells were incubated with Pronase (Roche) to a final concentration of 3 mg/mL for 10 min at 37 °C. To stop the reaction, phenylmethylsulfonyl fluoride (PMSF) was added to a final concentration of 100 μM and the mixture was rapidly cooled on ice. The protoplasts were centrifuged at 23,700 × *g* for 12 min at 4 °C. For the preparation of crude vesicles the protoplasts were suspended in vesicle buffer (40 mM potassium phosphate buffer, pH 7, containing 25 mM $MgSO_4{\cdot}7H_2O$, 0.4 mM sucrose, 10 mM DTE, and 1 mg/L resazurin) supplemented with 100 μM PMSF and a few crystals of DNase. The suspension is pressed through a French pressure cell at 400 PsiG. Remaining protoplasts as well as cell debris was removed by centrifugation (4,000 × *g*, 10 min, 4 °C). The supernatant is referred to as crude vesicle preparation.

**Artificial Energization of Inside-Out Membrane Vesicles.** To test whether the inside-out membrane vesicles (IMVs) were bioenergetically intact, an artificial pH gradient was applied, established by an ammonium diffusion potential. The preparation of the washed membrane vesicles was as described above, but the buffer for cell disruption and washing of the membrane vesicle was changed to a 20 mM potassium phosphate buffer, pH 6, containing 20 mM $MgSO_4{\cdot}7H_2O$, 0.4 M sucrose and 0.5 M $NH_4Cl$. Next, 5–20 μL of vesicle preparation was diluted into 2.5 mL of 20 mM potassium phosphate buffer, pH 6, containing 20 mM $MgSO_4{\cdot}7H_2O$, 0.4 M sucrose, 0.5 M choline chloride, and 1 μM acridine orange (5). Fluorescence was measured in a cuvettete in a fluorescence spectrophotometer (F-4500; Hitachi) with excitation at 470 nm and emission at 530 nm. The IMVs maintained a pH gradient >2.3 for 10–15 min, depending on the preparation.

**Measurement of ATP Synthesis.** Crude vesicles were diluted in 300 μL vesicle buffer (40 mM potassium phosphate buffer, pH 7, containing 25 mM $MgSO_4{\cdot}7H_2O$, 0.4 mM sucrose, 10 mM DTE, and 1 mg/l resazurin) to a final protein concentration of 25–30 mg/mL. The vesicles were preincubated for 10 min at 37 °C in 3.5-mL glass vials and then samples were taken as indicated in the figure legends. ATP synthesis was started by the addition of 20 mM methanol. Inhibitors were incubated with the vesicles for 20 min prior the experiment. ATP was determined by the luciferin-luciferase system as described before (6).

**Measurement of ATP Hydrolysis.** The experiments were performed under aerobic conditions in a buffer containing 25 mM Pipes-KOH buffer, pH 7, 25 mM $MgSO_4{\cdot}7H_2O$, and 0.4 M sucrose at 37 °C. For the experiments at different pH values, 25 mM Pipes-KOH/Mes-HCl buffer containing 25 mM $MgSO_4{\cdot}7H_2O$ and 0.4 M sucrose was used. One milliliter of buffer was supplemented with 17 μM valinomycin, 40 mM KCl, 10 mM $KHSO_3$, and NaCl, as indicated and combined with 30–60 μL of the washed vesicle preparation and incubated for 10 min at 37 °C. The $Na^+$ concentration was adjusted with NaCl. To start the reaction, 2.5 mM $K_2$-ATP was added and 200 μL of sample were taken every 2 min. Phosphate release was measured as described previously (7).

**Structural Modeling of $Na^+$- and $H^+$-Bound $c_4$ Oligomers.** Structural models of $c_4$ partial rings from the *M. acetivorans* ATP synthase were generated on the basis of known atomic structures of sequence-homologous *c* rings from other organisms. First, the structure of a single *M. acetivorans c* subunit was modeled based on the C-terminal hairpin of the *c* subunit from *Enterococcus hirae* (residues 92–156); this appears to be the most suitable template upon inspection of a multiple-sequence alignment of *c* subunits of known atomic structure (Fig. S3), obtained with T-Coffee (8). Two-thousand models were generated with Modeler 9v8 (9), from which the model with the best discrete optimized protein energy (DOPE) score (10) was selected. From this individual *c* subunit, two approximate models of a $c_4$ oligomer were constructed based on two distinct *c* ring architectures, namely that of the $Na^+$-bound $c_{11}$ ring from *Ilyobacter tartaricus* and that of the $H^+$-bound $c_{15}$ ring from *Spirulina platensis*. These $c_4$ models were obtained by iteratively superimposing the structure of the *M. acetivorans c* subunit onto consecutive *c* subunits in the full rings, according to a secondary-structure matching algorithm (11). Each of these crude $c_4$ oligomers was then used as a template to generate a new set of 50 models, either for the $c_{11}$- or $c_{15}$-like architecture, again using Modeler. The top-ranking model in each group was identified based on simultaneous GA341 (12) and DOPE scores. Side-chain configurations in the resulting models, which are either $Na^+$- or $H^+$-bound, were further optimized with backbone-constrained 1-ns molecular dynamics simulations *in vacuo*, using GROMACS 4.5 (13). Analogous $c_4$ oligomers were obtained directly from the crystal structures of the complete *c* rings from *I. tartaricus*, *B. pseudofirmus* OF4, and *S. platensis* (PDB entries 2WGM, 2X2V, and 2WIE, respectively), so as to be able to compare directly their $H^+/Na^+$ selectivity with that computed for *M. acetivorans*.

**Molecular Dynamics Simulations and Free-Energy of Selectivity Calculations.** All $c_4$ constructs ($Na^+$- and $H^+$-bound from *M. acetivorans*, $Na^+$-bound from *I. tartaricus*, $H^+$-bound from *S. platensis* and *B. pseudofirmus* OF4) were embedded in a hydrated palmitoyloleoylphosphatidylcholine (POPC) membrane (122–124 lipid molecules and ∼7,560 water molecules), using GRIFFIN (14). The $Na^+$-bound $c_4$ oligomers from *I. tartaricus* and *M. acetivorans* include a $Na^+$ ion coordinated by the conserved carboxylate side-chain ($Glu^{65}$ and $Glu^{66}$, respectively) in each of the *c-c* interfaces; in the *c* subunit exposed to the lipid membrane, this Glu side-chain is protonated. In the $H^+$-bound $c_4$ oligomers from *S. platensis, B. pseudofirmus* OF4, and *M. acetivorans*, the conserved Glu ($Glu^{62}$, $Glu^{54}$, and $Glu^{66}$, respectively) is protonated in

all subunits. $Glu^{37}$ is also protonated in both the $Na^+$- and $H^+$-bound *M. acetivorans* $c_4$ oligomers, by analogy with the equivalent $Gln^{32}$ and $Gln^{29}$ in *I. tartaricus* and *S. platensis*, respectively. All protein-membrane systems were equilibrated using all-atom molecular dynamics simulations, following a procedure whereby the dynamical range of the protein is gradually unrestricted over 2.5 ns. The final configurations of the $c_4$ constructs after equilibration were used as input of the free-energy calculations of $H^+$/$Na^+$ selectivity.

In these simulations, one of the ions is gradually transformed into the other (in both directions), and the associated energy change in the molecular system, $\Delta G_{site}$, is recorded. It can be shown that this free-energy change is related to the ratio of the dissociation constants of $Na^+$ and $H^+$, and therefore the chemical selectivity $\Delta G_{sel}$ (15):

$$\Delta G_{site} = \Delta G_{hyd} - k_B\, T \log \frac{K_d(Na^+)}{K_d(H^+)} = \Delta G_{hyd} + \Delta G_{sel},$$

where $\Delta G_{hyd}$ denotes the relative free-energy of hydration of the two ions. The difference in selectivity $\Delta\Delta G_{sel}$ between the binding sites of two rotors of different structure and amino acid sequence is therefore equal to the computed value of $\Delta\Delta G_{site}$.

These calculations were carried out using an alchemical-perturbation approach, in which the bound $Na^+$ is vanished (or created) while the coordinating carboxylate side-chain is transformed from the charged to the protonated state (or vice versa). Only the ion in the central site in the $c_4$ construct was exchanged. Each transformation is carried out in the context of a molecular dynamics simulation analogous to those described above. All free-energy perturbation calculations were carried out in the forward and backward directions, in 32 intermediate steps; each step amounts to 500 ps of simulation, including 100 ps of initial equilibration.

All simulations were carried out with NAMD 2.7 (16) using the CHARMM27 force-field for proteins and lipids (17, 18). The simulations were carried out at constant pressure (1 atm) and temperature (T = 298 K), imposed with a Nosé-Hoover Langevin barostat and thermostat. The dimensions of the simulation box in the plane of the membrane (48 × 94 Å) were also constant, but periodic-boundary conditions were used in all directions. Electrostatic interactions were calculated using Particle-Mesh Ewald with a real-space cutoff of 12 Å. A cutoff distance of 12 Å was also used for van der Waals interactions. Center-of-mass constraints were applied on the $c_4$ constructs to keep them appropriately centered and oriented within the simulation box; the $c_4$ assemblies, however, could tumble freely within the lipid membrane. During the free-energy calculations, the conformation of the first and last subunits in each of the $c_4$ constructs (i.e., those facing the lipid) was also constrained using a weak harmonic potential acting on the rmsd of the Cα-trace, relative to the initial structure. No restrictions were imposed on the structure and dynamics of the $c$ subunits flanking the perturbed binding sites, which can therefore freely adapt to either the bound $H^+$ or $Na^+$.


1. Sowers KR, Baron SF, Ferry JG (1984) *Methanosarcina acetivorans* sp. nov., an acetotrophic methane-producing bacterium isolated from marine sediments. *Appl Environ Microbiol* 47:971–978.
2. Pritchett MA, Zhang JK, Metcalf WW (2004) Development of a markerless genetic exchange method for *Methanosarcina acetivorans* C2A and its use in construction of new genetic tools for methanogenic archaea. *Appl Environ Microbiol* 70:1425–1433.
3. Sowers KR, Boone JE, Gunsalus RP (1993) Disaggregation of *Methanosarcina* spp. and growth as single cells at elevated osmolarity. *Appl Environ Microbiol* 59:3832–3839.
4. Metcalf WW, Zhang JK, Shi X, Wolfe RS (1996) Molecular, genetic, and biochemical characterization of the *serC* gene of *Methanosarcina barkeri* Fusaro. *J Bacteriol* 178: 5797–5802.
5. Peinemann S, Blaut M, Gottschalk G (1989) ATP synthesis coupled to methane formation from methyl-CoM and $H_2$ catalyzed by vesicles of the methanogenic bacterial strain Gö1. *Eur J Biochem* 186:175–180.
6. Becher B, Müller V (1994) $\Delta\mu_{Na^+}$ drives the synthesis of ATP via an $\Delta\mu_{Na^+}$-translocating $F_1F_0$-ATP synthase in membrane vesicles of the archaeon *Methanosarcina mazei* Gö1. *J Bacteriol* 176:2543–2550.
7. Heinonen JK, Lahti RJ (1981) A new and convenient colorimetric determination of inorganic orthophosphate and its application to the assay of inorganic pyrophosphatase. *Anal Biochem* 113:313–317.
8. Notredame C, Higgins DG, Heringa J (2000) T-Coffee: A novel method for fast and accurate multiple sequence alignment. *J Mol Biol* 302:205–217.
9. Fiser A, Sali A (2003) Modeller: Generation and refinement of homology-based protein structure models. *Methods Enzymol* 374:461–491.
10. Shen MY, Sali A (2006) Statistical potential for assessment and prediction of protein structures. *Protein Sci* 15:2507–2524.
11. Ortiz AR, Strauss CEM, Olmea O (2002) MAMMOTH (matching molecular models obtained from theory): An automated method for model comparison. *Protein Sci* 11: 2606–2621.
12. Melo F, Sali A (2007) Fold assessment for comparative protein structure modeling. *Protein Sci* 16:2412–2426.
13. Hess B, Kutzner C, van der Spoel D, Lindahl E (2008) GROMACS 4: Algorithms for highly efficient, load-balanced, and scalable molecular simulation. *J Chem Theory Comput* 4:435–447.
14. Staritzbichler R, Anselmi C, Forrest LR, Faraldo-Gómez JD (2011) GRIFFIN: A versatile methodology for optimization of protein-lipid interfaces for membrane protein simulations. *J Chem Theory Comput* 7:1167–1176.
15. Krah A, et al. (2010) Structural and energetic basis for $H^+$ versus $Na^+$ binding selectivity in ATP synthase $F_o$ rotors. *Biochim Biophys Acta* 1797:763–772.
16. Phillips JC, et al. (2005) Scalable molecular dynamics with NAMD. *J Comput Chem* 26: 1781–1802.
17. MacKerell AD, et al. (1998) All-atom empirical potential for molecular modeling and dynamics studies of proteins. *J Phys Chem B* 102:3586–3616.
18. Mackerell AD, Jr., Feig M, Brooks, CL, 3rd (2004) Extending the treatment of backbone energetics in protein force fields: limitations of gas-phase quantum mechanics in reproducing protein conformational distributions in molecular dynamics simulations. *J Comput Chem* 25:1400–1415.

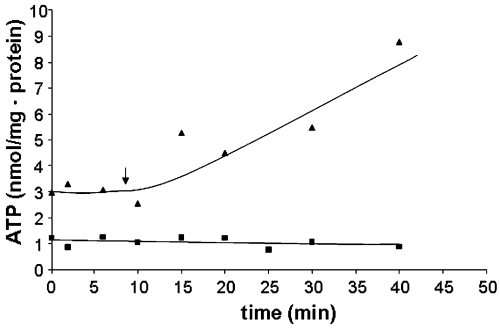


**Fig. S1.** MeOH dependent ATP synthesis of crude vesicles. Crude vesicles (300 μL, final protein concentration 26 mg/mL) were incubated at 37 °C in a shaking water bath. At the time point indicated (arrow), 20 mM MeOH were added. One assay (■) was preincubated with dicyclohexylcarbodiimide (620 μM).

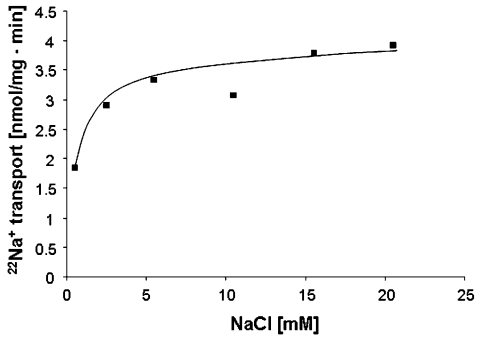


**Fig. S2.** Effect of increasing $Na^+$ concentrations on $Na^+$ transport. Washed membrane vesicles (final concentration 0.91 mg/mL) were incubated in 1 mL of 25 mM Pipes-KOH buffer, pH 7, containing 25 mM $MgSO_4 \cdot 7H_2O$ and 0.4 M sucrose. The assay was supplemented with 17 μM valinomycin, 10 mM $KHSO_3$, and 40 mM KCl and increasing $Na^+$ concentrations. The $Na^+$ concentration of the assay without additional $Na^+$ was 0.46 mM.

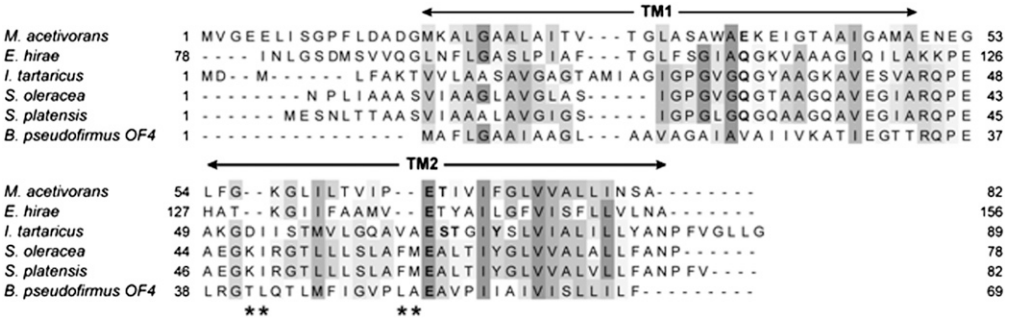


**Fig. S3.** Alignment of the sequence of the *M. acetivorans c* subunit against *c* subunit sequences of known atomic structure. The putative transmembrane helices in the *M. acetivorans c* subunit (TM1, TM2) are indicated; residues involved in ion binding are highlighted in bold. The alignment reveals two insertions (of two residues each, indicated by asterisks) in TM2 of *M. acetivorans*, with respect to the sequences of the F-type ATP synthases (*I. tartaricus*, *Spinacia oleracea*, *S. platensis*, and *Bacillus pseudofirmus* OF4). We therefore reasoned that the *c* subunit from the V-type ATPase from *E. hirae*, and in particular the C-terminal hairpin (TM3 and TM4), is the most suitable template of known structure for homology-modeling the single *M. acetivorans c* subunit. The sequence of *E. hirae* is also the second most similar, with 30% identity (compare with 20%, 27%, 24%, and 34% for *I. tartaricus*, *S. oleracea*, *S. platensis*, and *B. pseudofirmus* OF4, respectively).